Amygdala and Insula Connectivity Changes Following Psychotherapy for Posttraumatic Stress Disorder: A Randomized Clinical Trial

Supplemental Information

Supplemental Methods

Participants and Assessments

Individuals, between the ages of 18-65, were recruited by advertisement for participation in a psychotherapy treatment study for survivors of trauma in an academic medical center. After receiving a full explanation of study procedures, participants provided written informed consent for study participation. Trained PhD-level clinicians established DSM-IV diagnoses using the Clinician-Administered PTSD Scale for PTSD (CAPS) (1) and the Structured Clinical Interview for DSM-IV Diagnosis for non-PTSD diagnoses (SCID-IV) (2). The “2 for intensity/1 for frequency” scoring rule was utilized to establish whether or not a symptom criterion was met for the establishment of diagnosis (3). See our prior publications for additional information on other symptom measures collected (4, 5). Participants with comorbid mood and anxiety disorders secondary to PTSD were included, as well as those with a history of substance dependence if abstinence had been maintained for more than three months. Regular psychotropic medication use was permitted only for antidepressant medication (5 participants used regular selective serotonin reuptake inhibitors throughout the duration of the study) as long as the participant was stable on the same dosage, frequency, and type of medication for at least 3 months. No other regular psychotropic medications were allowed. As-needed use of benzodiazepines as allowed up to three times per week and not within 48 hours of a scan, which was verbally verified by clinician or study team

member. Other types of psychotropic medications such as mood stabilizers, antipsychotics, or anticonvulsants were not permitted, nor were regular use of thyroid medications or opiates. Participants were not allowed to have had any prior experience of prolonged exposure treatment, and no more than three sessions of any exposure-based psychotherapy. More extensive prior psychotherapy, i.e. more than 3 sessions, was allowable as long as it did not involve therapeutic exposure. This information was collected from the participant via self-report during the screening phase of the study.

General Inclusion and Exclusion Criteria

Inclusion criteria for all participants encompassed the following: eligibility for scanning (i.e., no metal embedded in body, not currently pregnant, no history of severe claustrophobia), good English comprehension, currently meeting criteria for a PTSD diagnosis, and intellectual function adequate for comprehension of experimenter instructions. Exclusion criteria for all participants included: lifetime diagnosis of psychosis, bipolar disorder, intellectual disability, neurodevelopmental disorders, history of neurological conditions or organic mental disorder (e.g., stroke, seizures, tumor, intracranial hemorrhage, multiple sclerosis), and substance dependence within the past three months.

MRI Data Acquisition

Images were acquired on a 3-T GE Signa scanner using a custom-build head coil. During the resting state scan, twenty-nine slices (4.0 mm thickness, 0.5 mm gap) were acquired in the axial direction across the whole brain using a T2*-weighted

gradient echo spiral pulse sequence (TR = 2000 ms, TE = 30 ms, flip angle = 80°, 1 interleaf, field of view = 22 cm, 64x64 matrix) sensitive to the blood oxygenation level dependent (BOLD) response. A high-resolution T1-weighted image (three-dimensional inversion recovery spoiled gradient-recalled acquisition in the coronal place with the following parameters: inversion time = 300 ms, TR = 8 ms, TE = 3.6 ms, flip angle = 15°, field of view = 22 cm, 124 slices, matrix = 256x192, number of excitations = 2, acquired resolution = 1.5 x 0.9 x 1.1 mm) was likewise obtained for each participant. Measures of heart rate and respiration were also collected and used to remove physiological noise from the BOLD time series (6).

Randomization

Following completion of baseline clinical assessments and fMRI scan, participants were individually randomized to one of two arms: 1) Immediate treatment with prolonged exposure therapy; or 2) Treatment waitlist. This occurred using random selection of a number from the string of digits 1 to 10, within an even selection indicating assignment to immediate treatment and an odd selection indicating assignment to waitlist. This randomization was performed by study staff and was always witnessed/supervised by one of the senior study personnel. A total of sixty-six (N=66) individuals were randomized, with 36 being randomized to immediate treatment, and 30 to treatment waitlist. If randomized to immediate treatment, participants commenced treatment with a clinical psychologist trained to deliver prolonged exposure therapy. If randomized to waitlist, individuals were instructed they would have a 10-week waiting period after which they would undergo a second clinical assessment and fMRI scanning

session. After completion of this second assessment, individuals on treatment waitlist were then assigned to a study therapist for completion of prolonged exposure therapy, which was provided for ethical reasons and not for neuroimaging analyses (since this would be outside of the randomized trial context).

Treatment Frequency and Length

Treatment sessions occurred on either a once or twice-weekly basis, for a total of either 9 or 12 90-minute sessions, according to manualized procedures (7). We chose to utilize a flexible treatment frequency format and allow for either once or twice-weekly sessions in order to reduce participant burden and minimally disrupt the participants' existing scheduled commitments. The variable duration of treatment (9 or 12 sessions) was utilized in order to ensure that each participant received the maximal therapeutic benefit from prolonged exposure while also allowing for inter-individual differences in rate of therapeutic responses, which has been previously employed in similar treatment outcome designs (8).

At sessions 2, 4, 6, and 8 individuals were administered the PTSD-Checklist Civilian Version for DSM-IV (PCL-C) (9) as well as the Beck Depression Inventory-II (BDI-II) (10) to track response to treatment. The benchmark used to establish adequacy of treatment response at Session 9 and subsequent termination was a reduction in Session 8 PCL-C scores to less than 30% of the PCL-C total score at intake (i.e. 70% reduction from baseline) (8). If individuals met this benchmark, they were given the option to discontinue treatment after Session 9. If individuals did not meet this benchmark and/or wished to continue for an additional 3 sessions, treatment was

terminated after Session 12. If treatment continued to 12 sessions, PCL and BDI measures were administered at Sessions 10 and 12.

Therapist Competency and Supervision in Prolonged Exposure

All psychologists received training in delivery of prolonged exposure and were deemed to meet competence in delivery of the treatment by one of the treatment developers, consultant to the study, and clinician supervisor Barbara Rothbaum, Ph.D. Dr. Rothbaum provided weekly group supervision to study therapists and reviewed video recordings of treatment sessions to rate compliance with the treatment protocol and to provide supervision. Dr. Rothbaum watched the entirety of the first three treatment sessions for each therapist to ensure therapist familiarity and competence with all major components of the treatment (all delivered in the first three sessions), and she continued to review relevant portions of remaining sessions as directed by study therapists. All study therapists demonstrated good compliance with the therapy protocol and with no significant deviations, as demonstrated by good-to-excellent supervisor ratings of treatment session adherence.

Treatment Structure

Prolonged exposure therapy was delivered according to manualized procedures (7). All sessions were audio recorded on a digital voice recorder (entrusted to the participant to take home with them and for use in completing imaginal exposure homework assignments) as well as a digital video recorder (for the purposes of assessing treatment adherence, therapist competency, and clinical supervision). In

brief, the structure and progression of treatment is as follows. Session 1 consisted of psychoeducation on posttraumatic stress disorder symptoms, the rationale for treatment, and treatment structure. It also involved additional assessment by the therapist of trauma history (including the index trauma, already established at intake), current symptoms, and current impairment. Breathing retraining was taught at the end of Session 1 and practiced collaboratively in session, which consisted of a normal inhalation and a controlled and slow exhalation with internal repetition of a calming word or phrase (e.g., “Calm”) and a pause between exhalation and next inhalation, which was audiotaped for the participant. Session 2 consisted of homework review, self-report measures, a discussion of common reactions to trauma, a rationale for exposure as a treatment tool, construction of an exposure hierarchy for *in-vivo* exposure exercises, and selection of 2 to 3 hierarchy items for homework practice. Session 3 involved homework review, a brief rationale for imaginal exposure, and the first imaginal exposure in session for 45-60 minutes. This was followed by a processing portion in which the therapist and participant discussed the participant’s experience of the exposure, any insights received through that process, and areas to be further addressed in future exposures. Homework was then assigned (including completion of in-vivo exposures and imaginal exposures daily and practice of breathing retraining). Session 4 consisted of the same format as Session 3 but without the discussion of rationale for imaginal exposure. Beginning in Session 5, the concept of trauma memory “hotspots” was discussed with participants, which were points in the memory during which the participant experienced the highest level of distress. The in-session imaginal exposure began to shift towards emphasizing hotspots in the memory in Session 5, at

earliest, and sometimes Session 6 if agreed to be clinically appropriate by the participant and therapist. Sessions 6, 7, and 8 involved a similar format, with homework review, imaginal exposure to hot spots, processing, and homework assignment. For participants reaching the PCL clinical benchmark in Session 8, and agreeing to end in 9 sessions, Session 9 consisted of homework review, a brief imaginal exposure of the entire trauma memory conducted in-session (20-30 minutes), a brief processing, and a final review of treatment progress and skills acquired. For participants not reaching the clinical benchmark and/or wishing to continue for an additional 3 sessions, Sessions 9-11 maintained the same format as Sessions 4-8. In this case, Session 12 served as the final session (which assumed the aforementioned format).

Primary and Secondary Outcomes

All primary and secondary outcomes were assessed prior to randomization and approximately 1 month following the cessation of treatment or waiting list. The specified primary outcome measure for the study was the total score from the Clinician-Administered PTSD Scale for DSM-IV (1), which assessed the degree of PTSD symptom change from pre- to post-treatment. The results of this outcome have been previously reported (4, 5). Secondary outcomes included the 30-item short form version of the Mood and Anxiety Symptom Questionnaire (11), including the General Distress, Anhedonic Depression, and Anxious Arousal subscales (reported in Table 1); fMRI-assessed resting connectivity (reported in this manuscript); and behavioral and neural implicit emotion regulation as assessed by an emotional conflict task (previously reported) (4, 5).

Post-Treatment Assessments

Approximately 4 weeks following the final treatment session (or 10 weeks following the beginning of treatment waitlist), participants completed a post-treatment/post-waiting list clinical assessment. A 4-week period was chosen to intercede between final session and post-treatment assessment in order to allow treatment changes to consolidate and symptom levels to equilibrate and to not overlap with the treatment period in assessing past-month PTSD symptoms. Moreover, brain changes from baseline noted as this time delay will be more representative of those changes conveying long-term therapeutic improvements. Participants were administered the CAPS and SCID again at post-treatment to assess change in PTSD symptoms and comorbid diagnoses. After completing the post-treatment clinical assessments, participants returned on a separate day to complete the post-treatment fMRI scan, which was identical to that of the pre-treatment session.

Sample Size Considerations

An *a priori* power analysis based upon effect size estimates for prolonged exposure on symptom and brain outcomes suggested that a randomized sample of 64 individuals would provide adequate power to detect moderate effect sizes with assumed power of 0.8 and $\alpha = 0.05$.

Resting State Connectivity Processing Pipeline

Resting state BOLD sequences were pre-processed and connectivity calculated on the individual level using the CONN toolbox version 15.h (12), which implemented

the SPM 12.0 software package within the Matlab R2019b software environment. The pre-treatment T1 structural image for each participant was defined as the session-invariant structural, while pre- and post-treatment resting state BOLD sequences were defined as separate sessions. The default pre-processing pipeline was utilized, which was included functional realignment and unwarping, centering of the functional and structural images to the stereotactic origin, structural segmentation and spatial normalization, functional spatial normalization, functional outlier detection utilizing the artifact rejection toolbox-based scrubbing, and functional smoothing with a 6.0 mm FWHM Gaussian smoothing kernel. Pre-processed mean BOLD time series signals were then extracted from subject-specific masks of white matter, gray matter, and cerebrospinal fluid (CSF). Covariates on the first-level were then defined for subsequent BOLD time series denoising, which included subject-specific white matter and CSF time series (no global signal regression), six rigid-body realignment parameters from the preprocessing stage, and a scrubbing regressor corresponding to the time series points to be removed from individual-level analysis. Quality control settings for artifact rejection tools (ART toolbox) corresponded to the “Intermediate” setting (97^{th} percentile), which flagged volumes with global signal changes > 5 SD above the mean and framewise displacement > 0.9mm. Additional quality control cutoffs instituted were: a) no more than 4mm root mean square absolute displacement across the mean of the squared maximum displacements in each of the 6 estimated translational and rotational motion parameters across the entire run; and b) no more than 5% (12 volumes) of the entire run flagged to be censored from analysis. The default denoising parameters in CONN were utilized and included the first 5 principal

components of each of the white matter and CSF time series (known as anatomical CompCor), the six rigid-body realignment parameters and their first-order derivatives, and single time point regressors corresponding to outlier time points to be removed from the analysis (known as the "scrubbing" covariate in CONN). Images were despiked and bandpass filtered following regression at a spatial frequency > 0.008 and < 0.1 and linearly de-trended. Covariates for denoising were also regressed out of the extracted seed region time series, as well as on a per-voxel basis for subsequent first-level analyses. Voxel wise analysis was conducted in the template (MNI space) with a 2mm isotropic voxel resolution on percent signal changes using an explicitly-defined brain mask. Preprocessed, denoised, and artifact-corrected mean BOLD time series within masks specifying *a priori* seed regions of interest (see section below), masked by the subject's own individual gray matter map, were extracted and then correlated for estimating functional connectivity (weighted GLM to derive bivariate correlations) on a seed to voxel basis. The confound-corrected voxelwise BOLD time series was exported for each subject and session, as were first-level seed to voxel *r* and *Z* brain maps.

Resting State Connectivity Seed Region Definitions

See Figure S1 for visual depiction of seed regions on the MNI152 average brain. Seed regions of interest were defined utilizing established and/or independently-defined anatomical or functionally-parcellated brain maps. For the amygdala, seed regions specifying amygdala subregions of the basolateral, centromedial, and superficial amygdala were defined utilizing the Juelich histological atlas probabilistic maps (13) in MNI standard space with a probabilistic threshold of no less than 40% likelihood of

assignment to one of the subregions and not another subregion or nearby structure. Specifically, the basolateral and centromedial divisions were thresholded at 70% probability, while the superficial amygdala was thresholded at a 40% probability, and all were then binarized. These percentages were chosen because they offered the strictest likelihood of assignment of amygdala voxels to one subregion of interest while also eliminating potential overlap between subregions (i.e. having one or more voxels assigned to more than one subregion) and continuing to maintain subregion external boundaries within the standardized amygdala MNI atlas definitions. Similar probabilistic thresholds have been utilized in other investigations for this purpose (14). Insula connectivity patterns were investigated utilizing functionally-defined parcellations derived from k-means clustering of resting state connectivity of all voxels within the insula with all other voxels in the brain, and further validated for specificity utilizing meta-analytic coactivation maps (15). This approach resulted in three insula unique subdivisions with unique co-activation patterns characterized by an anterior-posterior and a dorsal-ventral gradient: a ventral anterior insula, a dorsal anterior insula, and a posterior insula, which parallels results of other insular parcellations (16, 17). Coherence maps of each subdivision (all in the right insula, as this parcellation scheme was only implemented for one hemisphere) were retrieved from NeuroVault (www.neurovault.org) and were thresholded at 75% for each subdivision, as this threshold was found to best balance non-overlap of voxels across subregions with maintaining spatial extent of insular subdivisions consistent with stereotactic definitions, and then binarized. Left insula subdivisions were created by flipping these binarized

masks along the anterior-posterior axis of MNI space. This approach thus yielded six insula subdivisions total, with 3 in each hemisphere.

Seeded Connectivity Group Analysis

To examine treatment-related changes in seeded connectivity patterns, the seed connectivity maps for each anatomical structure's subregions (basolateral, centromedial, and superficial amygdala; posterior, ventral anterior, and dorsal anterior insula) were subjected to an intent-to-treat voxel wise linear mixed model conducted using AFNI's 3dLME package (18). At each voxel within an independently defined gray matter mask, connectivity values for each structure were modeled in separate analyses (for amygdala and insula) as a function of a random (allowing for individual variability in baseline connectivity) and fixed intercept and fixed effects of time, subregion, time x treatment arm, time x subregion, and time x subregion x treatment arm (and an additional set of main effects and interaction effects for hemisphere for the insula subdivisions, since these were derived from a parcellation scheme that incorporated a single hemisphere parcellation). The effects of interest were the interactions with treatment arm, specifying differences between prolonged exposure and waitlist in seeded connectivity change from pre-to-post treatment across all portions of the anatomical structure (time x treatment arm) and differential changes in connectivity between prolonged exposure and waiting list from pre- to post-treatment that were specific to a structure's subregion (time x treatment arm x subregion). The *F* statistical maps for each effect of interest were then corrected for multiple comparisons utilizing a whole brain voxel level false discovery rate (FDR) correction, yielding FDR-corrected Z

values that were then thresholded at a corrected $p < 0.025$. This posterior threshold is Bonferroni-corrected for the two sets of seeded connectivity analyses, yielding a modality-wise α of 0.05. Voxels surpassing this corrected threshold were then clustered for the purposes of extracting average connectivity values within each participant to visualize directionality of effects. Subsequent visualization of linear mixed model effects were conducted in IBM SPSS version 21 (19). Baseline presence of major depressive disorder (MDD) diagnosis was also explored as a potential moderator of treatment effects utilizing *post hoc* extractions from areas identified in the primary voxelwise analyses. For these exploratory analyses, an effects-coded variable specifying presence or absence of MDD diagnosis at baseline was specified in the context of a linear mixed model in IBM SPSS, and also in interaction with time, time x treatment arm, time x subregion, and time x subregion x treatment arm. The effects of interest here were the interactions of MDD diagnosis x time x treatment arm (specifying a differential effect for PE vs. WL on time-related connectivity changes as a function of baseline MDD diagnosis) and the MDD diagnosis x time x subregion x treatment arm (specifying a subregion-specific differential effect for PE vs. WL on time-related connectivity changes as a function of baseline MDD diagnosis).

Relationship of Amygdala and Insula Connectivity Changes to Symptom Changes

To examine relationships between common amygdala and insula connectivity changes and symptom changes, we tested in a linear mixed model framework whether the effect of treatment on CAPS total score changes was moderated by amygdala and insula connectivity changes with targets displaying significant and congruent treatment-

related increases or decreases in connectivity that were common across both the amygdala and insula subregion-general Type I error-corrected effects maps (identified via a *post-hoc* conjunction analysis). Subregional average connectivity values at pre and post-treatment were extracted from each participant in clusters identified by conjunction, and each was subjected to a mixed model analysis with a random intercept and fixed effects of time, time x treatment arm, connectivity change (post vs. pre-tx) x time, and time x treatment arm x connectivity change interaction. This latter interaction specifies the difference in the treatment effect on symptom changes from pre- to post-treatment as a function of connectivity change in each cluster, thereby providing an assessment of the continuous relationship between connectivity change magnitudes and symptom change magnitudes. Bonferroni-correction across all clusters from the conjunction analysis was utilized to control for Type I error inflation due to multiple comparisons, yielding a posterior cutoff of $p < 0.0016$ (two-sided p of 0.05 divided by 16, 8 tests each for the amygdala and insula).

DCM First-Level Analyses

DCM was conducted utilizing previously published methods and scripts (20). In brief, individual structural images and resting state functional data were preprocessed utilizing the processing pathway outlined in Almgren *et al.* (20). The five initial scan acquisitions from each run were discarded, and images then underwent slice timing correction (with the central slice as reference). Images were then realigned to the first volume in each session, were co-registered to the anatomical image, and then normalized to MNI space. Images were smoothed with a 6mm FWHM Gaussian

smoothing kernel. The *F* statistic from a GLM across a discrete cosine basis set (0.008 – 0.1 Hz, with the number of components being a function of the number of volumes and TR) was utilized to identify peaks of maximal low-frequency resting BOLD fluctuations in the amygdala and insula, controlling for 24 motion regressors (6 regressors representing instantaneous translations and rotations, 6 regressors representing motion on the prior volume, and the squares of both), and two nuisance regressors (cerebrospinal fluid signal from 5mm ROI in ventricles, white matter signal from 7mm ROI in brainstem). See Table S5 for the locations of these peak foci. Since the DCM model was deployed to interrogate directional influence between the amygdala and insula and targets displaying common intrinsic connectivity changes that scaled with symptom reductions, peaks were defined as the area of maximal magnitude of low frequency fluctuations in the left and right amygdala and insula as whole structures, i.e. not by subregion. This yielded four foci of interest (one each for the left and right amygdala and insula), as well as one focus in the left inferior frontal junction (IFJ) and one in the left intraparietal sulcus (IPS). Both the IFJ and IPS were identified in mixed model analyses as displaying significant treatment-related decreases in connectivity that were associated with treatment-related changes in symptoms for the amygdala and insula, respectively (Table S4). Time-series for these 6 nodes were extracted from each participant at each time point by identifying the individual's own subject-specific peak voxel within a 6mm radius of the group effect, and then defining a 6mm sphere for extraction around that peak voxel. Only voxels exceeding a $p < 0.05$ threshold were utilized for extracting the principal eigenvariate of the timeseries from the identified sphere. Fully-connected DCMs without exogenous input were then specified for each

subject at each time point, and the full models were inverted utilizing default shrinkage priors.

DCM Second-Level Analyses with Parametric Empirical Bayes

Inverted fully-connected models were then taken to second-level analyses with parametric empirical Bayes (PEB)(21) to: a) assess evidence for effective connectivity with the network at pre-treatment; and b) to assess treatment arm x time effects on effective connectivity parameters. For the former, a single regressor specifying the group mean at pre-treatment was entered into the analysis, and the fully-connected PEB was then estimated and subjected to Bayesian model reduction (BMR) (22) and Bayesian model averaging (BMA) (23) to determine the posterior free energies associated with the presence vs. absence of each parameter at the group level (24). For the latter analysis, time-related effects (post vs. pre-treatment) were specified for the PE and WL separately utilizing an intent-to-treat model with a regressor for the group mean and another specifying the mean-centered, effects-coded contrast of post vs. pre-treatment. These second-level PEBs were then estimated and carried to a third-level PEB analysis that examined the differences in time-related changes (treatment arm x time effects), specifying one mean regressor and another mean-centered, effects-coded regressor for PE vs. WL. This third-level PEB was then subjected to BMR and BMA to assess the posterior free energies for the presence vs. absence of the treatment arm x time effect on each model parameter at the group level.

To investigate how effective connectivity changes were associated with changes in PTSD symptoms in the prolonged exposure group in order to better ascertain which

changes might be adaptive, we conducted an additional PEB analysis in the PE group. We utilized mean-centered CAPS total scores (pre vs. post-treatment, for a positive scaling) in interaction with a time variable (post vs. pre-treatment) as a covariate of interest in a parametric empirical Bayes analysis, controlling for the main effects of time and the main effects of CAPS total score changes. This covariate identifies changes in effective connectivity that scale with treatment-related changes in symptoms.

Supplemental Results

Sample Characteristics

The study recruited from 2010-2016, and was stopped upon cessation of the funding period. The randomized sample encompassed 66 individuals, with 36 randomized to prolonged exposure treatment and 30 randomized to waiting list. Arms were well matched on all clinical and demographic variables (Table 1). At baseline, 18 in the PE group and 17 in WL met diagnostic criteria for MDD. Of those randomized, 25 individuals in the immediate treatment arm and 26 individuals in waiting list underwent post-treatment assessments. Of these, 1 individual randomized to prolonged exposure did not undergo a post-treatment resting state scan, which provided a total post-treatment imaging *N* of 50 (26 from waiting list, 24 from prolonged exposure). See prior publications from this study for further details on sample demographics, clinical characteristics, and treatment outcomes (4, 5). As expected, individuals randomized to PE displayed significantly larger reductions in PTSD symptoms from pre- to post-treatment relative to WL (Table 1). Individuals randomized to PE demonstrated significantly greater reductions in CAPS total scores relative to those randomized to WL ($F = 20.05$, $p < 0.001$), and this effect was due to more robust symptom improvement in the treatment group (parameter estimate = -36.87, $t = -8.90$, $p < 0.001$) relative to waitlist (parameter estimate = -6.64, $t = -2.16$, $p = 0.036$). Presence or absence of baseline MDD did not significantly moderate the PE vs. WL effect on PTSD symptom changes ($F = 2.77$, $p = 0.100$).

Motion Estimates and Imaging Quality Control

Head motion during the resting state fMRI scan was within acceptable parameters at all time points (<4mm root mean square absolute movement across the mean of the squared maximum displacements in each of the 6 estimated translational and rotational motion parameters; < 5% of volumes from the entire run flagged to be censored from analysis). At baseline, the average root mean square absolute displacement was 0.87 mm (SD = 0.82) and ranged from 0.13 to 3.90 mm. At post-treatment, the average root mean square absolute displacement was 0.68 mm (SD = 0.60) and ranged from 0.19 to 3.33 mm. There were no significant differences between groups in the mean or maximum displacements or rotations in the three dimensions at baseline (all *p's* > 0.08) or at post-treatment (all *p*'s > 0.07). The mean number of censored volumes at pre-treatment was 1.88 (SD = 2.06), while the median and mode were 2. Number of volumes censored ranged from 0 to 9, and the distributions did not differ between groups (t = -0.56, p = 0.58). At post-treatment, the mean number of censored volumes at was 1.79 (SD = 2.06), while the median and mode were 2. Number of volumes censored ranged from 0 to 10, and the distributions did not differ between groups (t = -0.45, p = 0.66).

Treatment-Related Effects on Intrinsic Connectivity

Amygdala

The intent-to-treat linear mixed model for amygdala connectivity patterns revealed a treatment arm x time effect (i.e. subregion-uniform treatment-specific changes) in widespread regions of the brain (Table S1 and Figure S3), but no significant

treatment arm x time x subregion connectivity effects (i.e. subregion-specific treatment-related changes). As hypothesized, we observed significant treatment arm x time effects on amygdala connectivity bilaterally with the ventral anterior insula (particularly prominent in the right hemisphere; Figure 1A), in the left posterior ventromedial prefrontal/orbitofrontal cortex (Figure 1B), and bilaterally in the anterior dorsolateral/frontopolar prefrontal cortices. The insula treatment arm x time effects were driven predominantly by increases in amygdala-anterior insula connectivity from pre- to post-treatment in the prolonged exposure arm, both in the right hemisphere (within-group trajectory change for prolonged exposure: $t = 2.69$, $p = 0.008$; waiting list: $t = -1.63$, $p = 0.11$) and left hemisphere (prolonged exposure: $t = 2.22$, $p = 0.027$; waiting list: $t = -0.62$, $p = 0.54$). The posterior ventromedial effect on the left side was also due to increases in connectivity in the prolonged exposure group ($t = 2.46$, $p = 0.014$) and a trend towards decreased connectivity in waiting list ($t = -1.48$, $p = 0.14$), and on the right side the interaction effect was driven by statistically significant increase in the treatment group ($t = 2.16$, $p = 0.034$) and a trend towards decreased connectivity in waiting list ($t = -1.64$, $p = 0.11$). An anterior portion of the dorsolateral prefrontal cortices bordering BA 10 in the right hemisphere also showed a treatment arm x time effect driven by increases in amygdalar connectivity from pre- to post-treatment in the prolonged exposure group (right hemisphere: $t = 2.10$, $p = 0.04$) as well as decreases in waiting list ($t = -2.06$, $p = 0.04$). More posterior dorsolateral prefrontal regions, however, showed the opposite pattern. For example, a treatment arm x time effect in the left inferior frontal junction (MNI center of mass: -46, 20, 31) was driven by significantly decreased amygdalar connectivity in the prolonged exposure arm ($t = -3.29$, $p = 0.001$) and no

change in waiting list (t = 0.22, p = 0.83), while an effect in the right hemisphere (MNI center of mass: 22, 28, 39) also displayed decreased connectivity in the prolonged exposure arm (t = -3.39, p = 0.001) and no change in waiting list (t = 1.28, p = 0.20). Other significant treatment arm x time effects included increased amygdala connectivity in the prolonged exposure arm post-treatment with the ventral visual cortex, the dorsal visual cortex (including calcarine gyri and cuneus), and bilaterally in the primary motor and sensory cortices. Additionally, the prolonged exposure arm also displayed decreases in amygdalar connectivity post-treatment with the posterior cingulate/precuneus, angular gyri, and the inferior parietal cortex. There were no significant moderating effects of MDD diagnosis in interaction with the treatment arm x time effect (all p's > 0.11) or the treatment arm x time x subregion effect (all p's > 0.32).

Insula

The voxel level treatment arm x time x subregion linear mixed model revealed a significant whole brain FDR-corrected treatment arm x time effect on insular connectivity patterns that was prominent and widespread (Table S2 and Figure S4), as well as significant treatment arm x time x subregion effects (Table S3). We focus first on describing the treatment arm x time effects that were not qualified by a significant subregional interaction (i.e. no significant treatment arm x time x subregion effect). As hypothesized, and confirming findings from the amygdala seeded connectivity analyses, we detected a treatment arm x time effect for insular connectivity in a large cluster encompassing the right amygdala (which also included the parahippocampal gyrus, striatum, and thalamus), with the prolonged exposure arm displaying significant

increases in connectivity (t = 5.07, p < 0.001) and waiting list displaying significantly decreased connectivity (t = -3.76, p < 0.001). A similar effect was noted in the left amygdala as part of a larger cluster encompassing the inferior temporal gyrus, parahippocampal gyrus, and hippocampus, with the prolonged exposure group displaying significantly increased connectivity (t = 2.51, p = 0.012) and the waiting list group displaying significantly decreased connectivity (t = -4.31, p < 0.001). Notably, an additional treatment arm x time effect for insular connectivity was observed in the left posterior ventromedial prefrontal cortex (cluster center of mass: -6, 15, -11), in an overlapping region demonstrating change with amygdala connectivity, and this effect was due to increases in connectivity in the prolonged exposure arm (t = 4.10, p < 0.001) and decreases in connectivity in waiting list (t = -2.92, p = 0.004) (Figure 1B). Increases in insular connectivity in the prolonged exposure arm were also observed more dorsally in the anteromedial frontopolar cortex in both hemispheres, more posteriorly in the right inferior frontal junction, in the ventral visual cortices, in the right posterior cingulate, cuneus, and bilaterally in the primary sensory and motor cortices. In contrast, decreases in insular connectivity in the prolonged exposure arm were observed in widespread portions of the cerebellum in both hemispheres, the precuneus, left parietal cortex, the left lateral frontopolar cortex, the rostrodorsal cingulate, the dorsomedial frontal gyri, and dorsolateral prefrontal cortical regions posterior to the frontopolar cortices but anterior to the inferior frontal junctions. There were no significant interactions of the treatment arm x time effect with hemisphere. There were no significant interactions of MDD diagnosis with the treatment arm x time effect (all *p's* > 0.09).

Treatment arm x time x subregion interaction effects were detected in several structures (Table S3), including the including the left motor/sensory cortices (increased connectivity of dorsal and posterior but not ventral insula for PE vs. WL); left supramarginal/angular gyri (decreased connectivity of dorsal and ventral but not posterior insula for PE vs. WL); right superior temporal gyrus (decreased connectivity of posterior but not dorsal or ventral insula for PE vs. WL); rostrodorsal anterior cingulate (decreased connectivity of posterior but not dorsal or ventral insula for PE vs. WL); right supplementary motor area (decreased connectivity of dorsal but not ventral or posterior insula for PE vs. WL); and right middle temporal gyrus (increased connectivity of posterior but not dorsal or ventral insula for PE vs. WL). There were no significant interactions of MDD diagnosis with the treatment arm x time x subregion effect (all *p's* > 0.17).

Effective Connectivity at Baseline

At pre-treatment, the DCM network demonstrated strong evidence (posterior probabilities (*Pp)* > 0.95; Table S6 and Figure 3A) for excitatory connections from each amygdala to the other; from each insula to the other; from the left insula to the left IFJ; and from the left IPS to the left IFJ. Strong evidence for inhibitory connections were observed from the amygdalae to the insulae and the left IPS; from the right amygdala to the left IFJ; from the left IFJ to the left and right amygdala and left and right insulae; and from the left IPS to the left and right insulae.

Supplemental References

1. Blake DD, Weathers FW, Nagy LM, Kaloupek DG, Gusman FD, Charney DS, et al. (1995): The development of a Clinician-Administered PTSD Scale. *Journal of traumatic stress*. 8:75-90.

2. First MB, Spitzer RL, Gibbon M, Williams JBW (2002): *Structured Clinical Interview for DSM-IV-TR Axis I Disorders, Research Version, Patient Edition (SCID-I/P)*. New York: Biometrics Research, New York State Psychiatric Institute.

3. Weathers FW, Ruscio AM, Keane TM (1999): Psychometric properties of nine scoring rules for the clinician-administered Posttraumatic Stress Disorder Scale. *Psychological Assessment*. 11:124-133.

4. Fonzo GA, Goodkind MS, Oathes DJ, Zaiko YV, Harvey M, Peng KK, et al. (2017): PTSD Psychotherapy Outcome Predicted by Brain Activation During Emotional Reactivity and Regulation. *Am J Psychiatry*. 174:1163-1174.

5. Fonzo GA, Goodkind MS, Oathes DJ, Zaiko YV, Harvey M, Peng KK, et al. (2017): Selective Effects of Psychotherapy on Frontopolar Cortical Function in PTSD. *Am J Psychiatry*. 174:1175-1184.

6. Glover GH, Li TQ, Ress D (2000): Image-based method for retrospective correction of physiological motion effects in fMRI: RETROICOR. *Magnetic resonance in medicine*. 44:162-167.

7. Foa EB, Hembree EA, Rothbaum BO, Rauch SA (2019): *Prolonged Exposure Therapy for PTSD: Emotional Processing of Traumatic Experiences*. Second ed. Oxford: Oxford University Press.

8. Foa EB, Hembree EA, Cahill SP, Rauch SA, Riggs DS, Feeny NC, et al. (2005): Randomized trial of prolonged exposure for posttraumatic stress disorder with and without cognitive restructuring: outcome at academic and community clinics. *Journal of consulting and clinical psychology*. 73:953-964.

9. Weathers F, Litz B, Herman D, Huska J, Keane T (1993): The PTSD Checklist (PCL): Reliability, Validity, and Diagnostic Utility. *Annual Convention for the International Society for Traumatic Stresss Studies*. San Antonio, TX.

10. Beck AT, Steer RA, Brown GK (1996): *Manual for the Beck Depression Inventory-II*. San Antonio, TX: Psychological Corporation.

11. Wardenaar KJ, van Veen T, Giltay EJ, de Beurs E, Penninx BW, Zitman FG (2010): Development and validation of a 30-item short adaptation of the Mood and Anxiety Symptoms Questionnaire (MASQ). *Psychiatry research*. 179:101-106.

12. Whitfield-Gabrieli S, Nieto-Castanon A (2012): Conn: a functional connectivity toolbox for correlated and anticorrelated brain networks. *Brain connectivity*. 2:125-141.

13. Amunts K, Kedo O, Kindler M, Pieperhoff P, Mohlberg H, Shah NJ, et al. (2005): Cytoarchitectonic mapping of the human amygdala, hippocampal region and entorhinal cortex: intersubject variability and probability maps. *Anatomy and embryology*. 210:343-352.

14. Etkin A, Prater KE, Schatzberg AF, Menon V, Greicius MD (2009): Disrupted amygdalar subregion functional connectivity and evidence of a compensatory network in generalized anxiety disorder. *Archives of general psychiatry*. 66:1361-1372.

15. Chang LJ, Yarkoni T, Khaw MW, Sanfey AG (2013): Decoding the role of the insula in human cognition: functional parcellation and large-scale reverse inference. *Cereb Cortex*. 23:739-749.

16. Deen B, Pitskel NB, Pelphrey KA (2011): Three systems of insular functional connectivity identified with cluster analysis. *Cereb Cortex*. 21:1498-1506.

17. Cauda F, D'Agata F, Sacco K, Duca S, Geminiani G, Vercelli A (2011): Functional connectivity of the insula in the resting brain. *Neuroimage*. 55:8-23.

18. Chen G, Saad ZS, Britton JC, Pine DS, Cox RW (2013): Linear mixed-effects modeling approach to FMRI group analysis. *Neuroimage*. 73:176-190.

19. IBM (2012): IBM SPSS Statistics for Macintosh, Version 21.0. Armonk, NY: IBM Corp.

20. Almgren H, Van de Steen F, Razi A, Friston K, Marinazzo D (2019): The effect of global signal regression on DCM estimates of noise and effective connectivity from resting state fMRI. *NeuroImage*.116435.

21. Zeidman P, Jafarian A, Seghier ML, Litvak V, Cagnan H, Price CJ, et al. (2019): A guide to group effective connectivity analysis, part 2: Second level analysis with PEB. *NeuroImage*.

22. Friston K, Penny W (2011): Post hoc Bayesian model selection. *NeuroImage*. 56:2089-2099.

23. Penny WD, Stephan KE, Daunizeau J, Rosa MJ, Friston KJ, Schofield TM, et al. (2010): Comparing families of dynamic causal models. *PLoS computational biology*. 6:e1000709.

24. Friston KJ, Litvak V, Oswal A, Razi A, Stephan KE, van Wijk BCM, et al. (2016): Bayesian model reduction and empirical Bayes for group (DCM) studies. *NeuroImage*. 128:413-431.

Figure S1. Seed regions utilized for connectivity analyses.

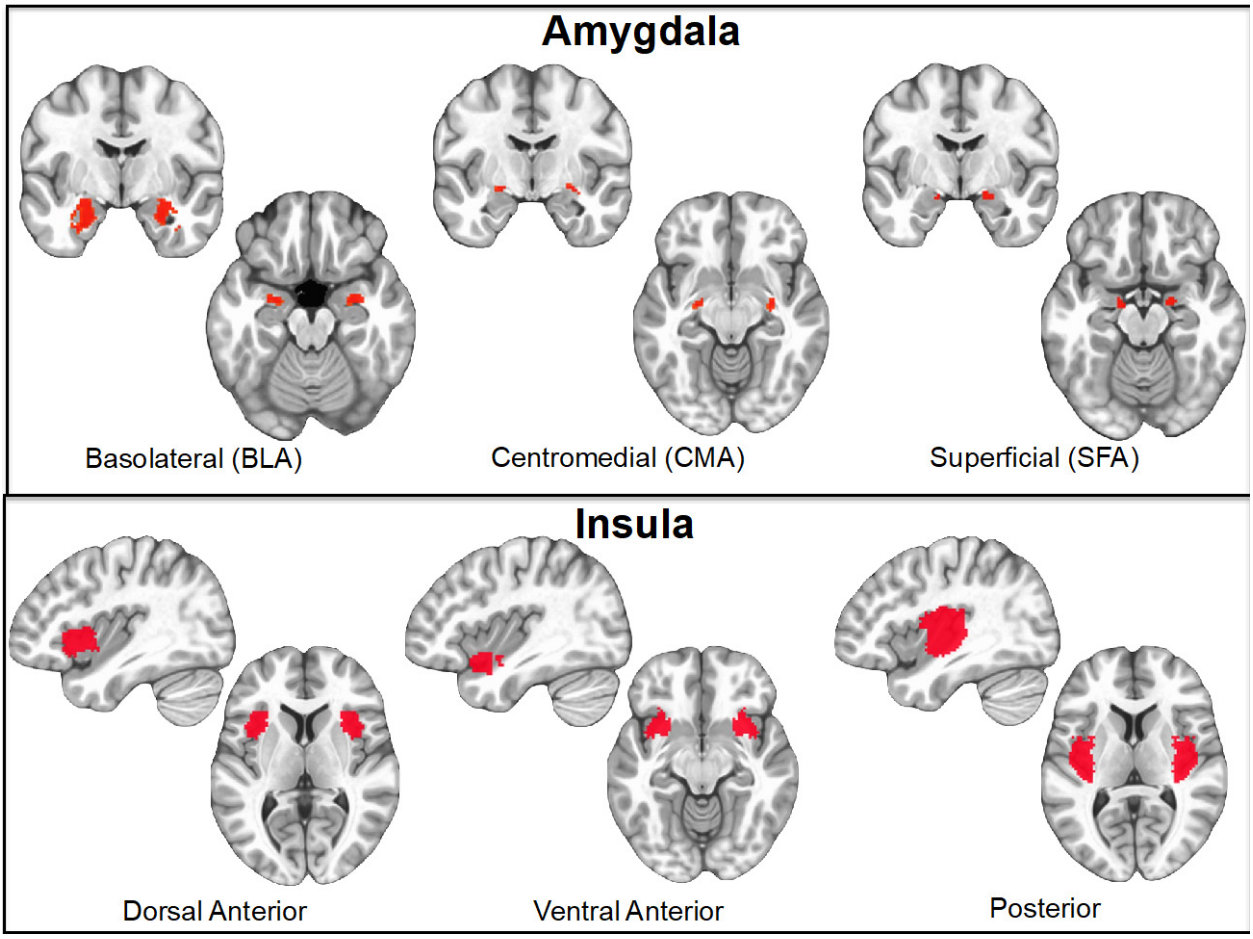

Figure depicts the volumetric masks of subregions of the amygdala and insula that were utilized for seeded connectivity analyses investigating voxel wise patterns of treatment-specific connectivity change. Seed regions are displayed on the MNI152 average anatomical.

Figure S2. CONSORT Flow Diagram.

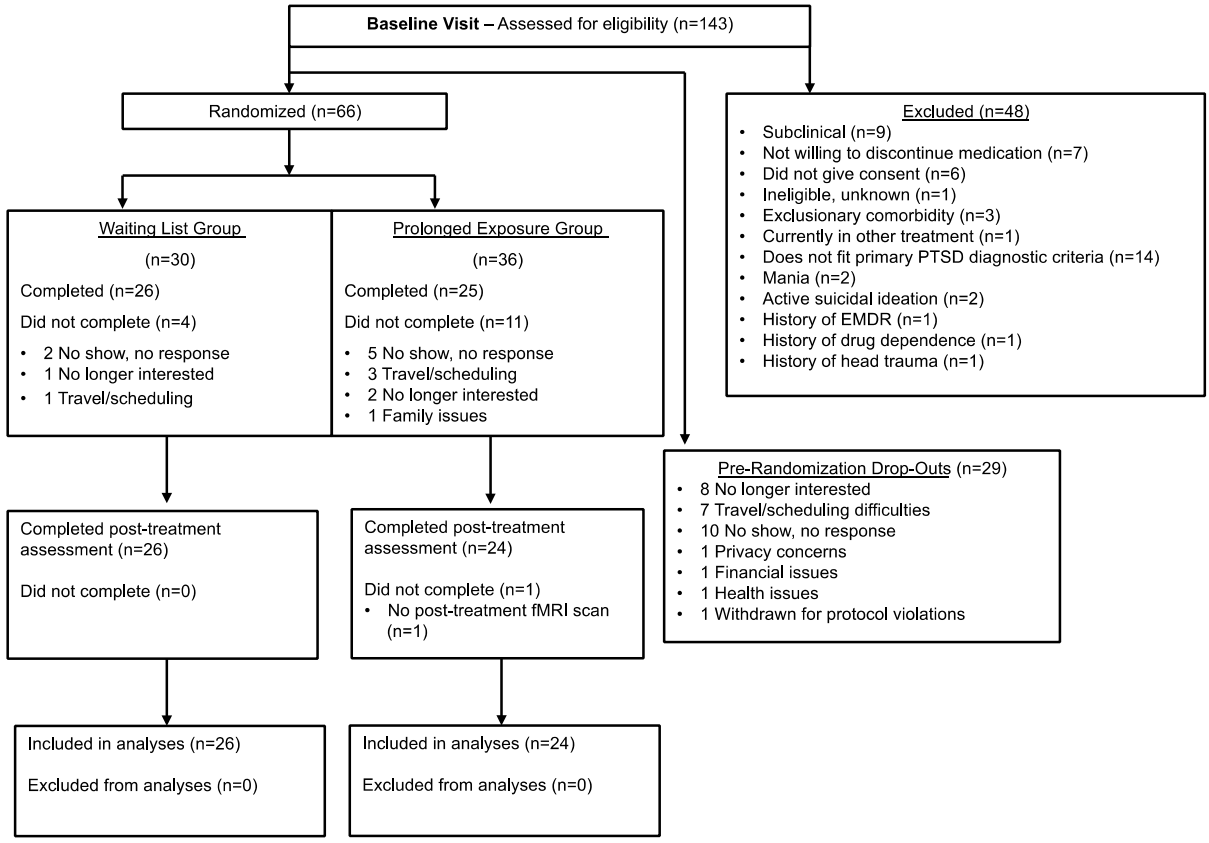

Figure depicts the flow of participants through the study, from initial eligibility assessment to the final analyses.

Figure S3. Treatment arm x time effect for amygdala seeded connectivity.

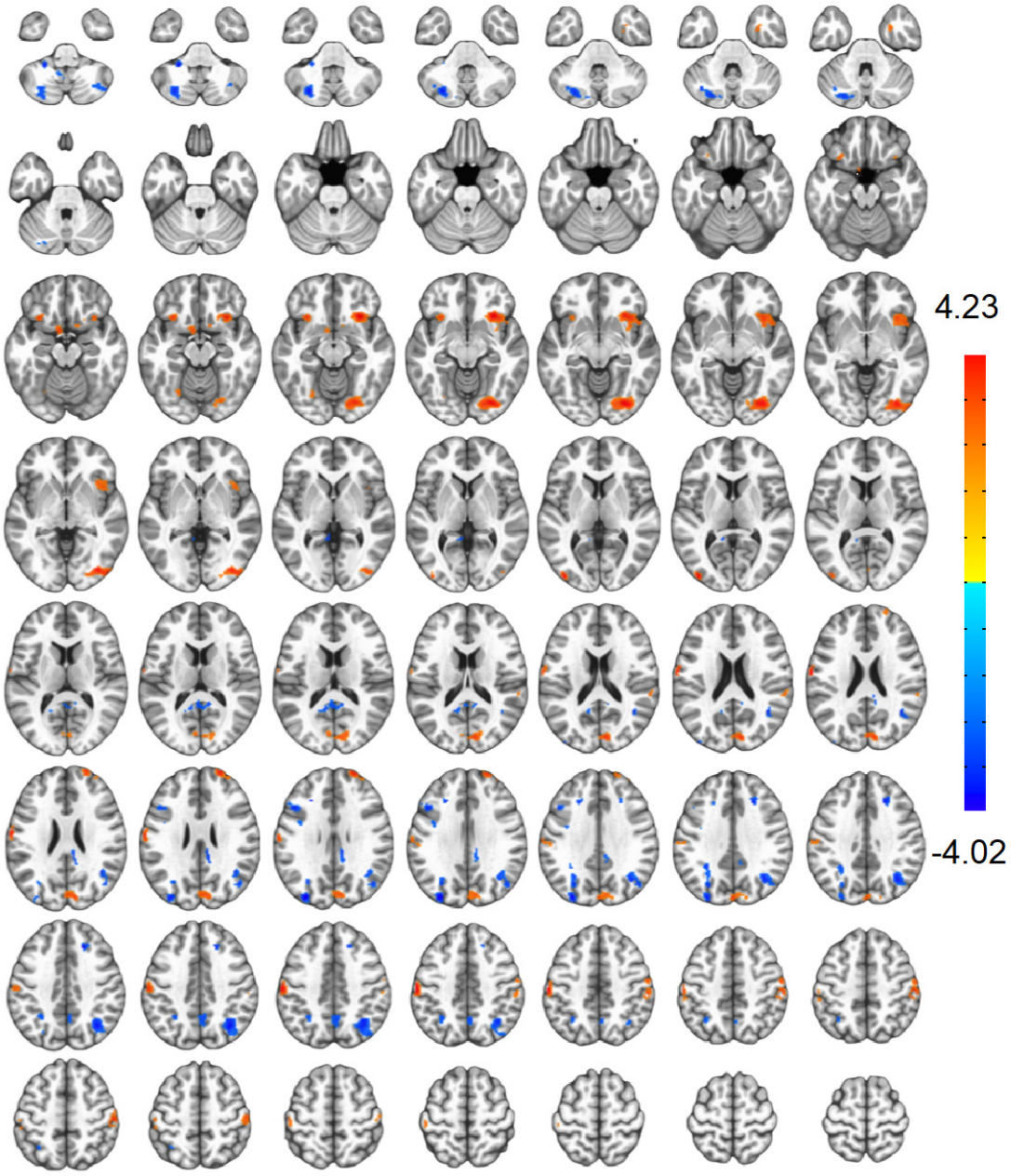

Axial montage depicts subregion-uniform changes (treatment arm x time interaction) for amygdala seeded connectivity. Effects are voxel-level FDR-corrected (FDR Z < 0.025) Z values for the treatment arm x time interaction with a sign (positive or negative) determined by the contrast of the post vs. pre-treatment comparison within the prolonged exposure arm (with positive values, i.e. warm colors, for areas displaying greater connectivity at post-treatment vs. pre-treatment, and negative values, i.e. cool colors, for areas displaying less connectivity at post-treatment vs. pre-treatment). Color bar indicates scale for FDR Z values, which are displayed on the MNI152 average anatomical.

Figure S4. Treatment arm x time effect for insula seeded connectivity.

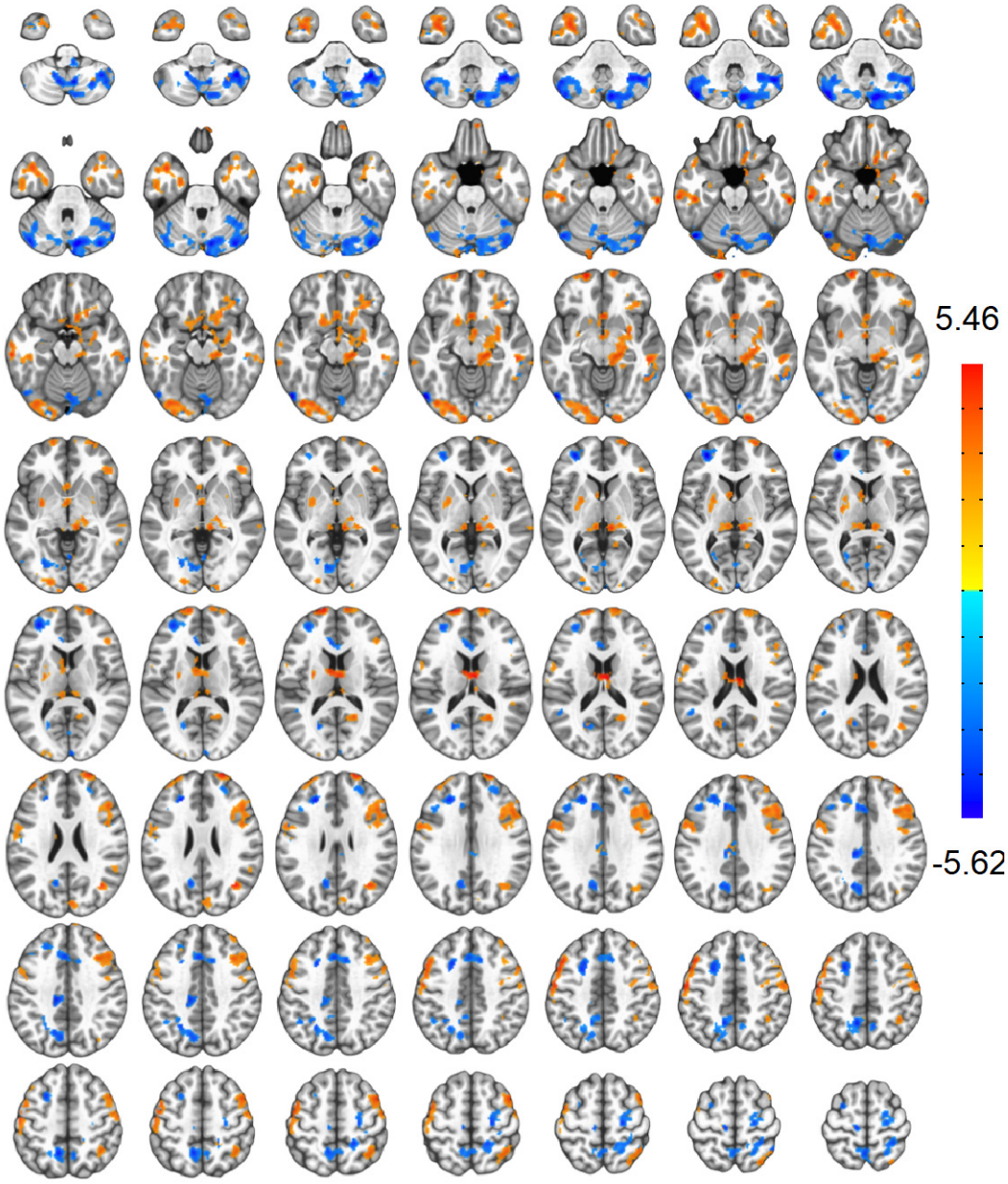

Axial montage depicts subregion-uniform changes (treatment arm x time interaction) for insula seeded connectivity. Effects are voxel-level FDR-corrected (FDR Z < 0.025) Z values for the treatment arm x time interaction with a sign (positive or negative) determined by the contrast of the post vs. pre-treatment comparison within the prolonged exposure arm (with positive values, i.e. warm colors, for areas displaying greater connectivity at post-treatment vs. pre-treatment, and negative values, i.e. cool colors, for areas displaying less connectivity at post-treatment vs. pre-treatment). Color bar indicates scale for FDR Z values, which are displayed on the MNI152 average anatomical.

Table S1. Differential Amygdala Connectivity Changes by Treatment Arm

Hem.	MNI Atlas Region(s)	# Voxels	X	Y	Z	Voxel Stats		Extractions		Predicted Connectivity (mean, SD)			
						FDR Z		*Parameter, Significance*		Pre		Post	
						Mean	*SD*	*PE*	*WL*	PE	WL	PE	WL
R	Inferior Occipital Gyrus/Lingual Gyrus/Middle Occipital Gyrus/Fusiform Gyrus/Calcarine Gyrus/Cerebellum	516	30	-81	-6	2.96	0.51	0.10, <0.001	-0.03, 0.042	0.04, 0.03	0.05, 0.03	0.11, 0.03	0.03, 0.03
R	Angular Gyrus/Superior Parietal Lobule/ Middle Occipital Gyrus/Inferior Parietal Lobule/Middle Temporal Gyrus/Superior Occipital Gyrus/Superior Temporal Gyrus	496	38	-63	37	2.70	0.35	-0.06, 0.004	0.05, 0.016	0.05, 0.04	0.02, 0.03	-0.01, 0.05	0.04, 0.03
R	Inferior Frontal Gyrus (p. Orbitalis)/Insula Lobe/Temporal Pole/Superior Orbital Gyrus/Middle Orbital Gyrus	410	35	19	-8	2.78	0.45	0.07, 0.008	-0.04, 0.11	0.08, 0.02	0.10, 0.02	0.11, 0.02	0.09, 0.03
L/R	Cuneus/Calcarine Gyri/Superior Occipital Gyri	349	6	-83	25	2.65	0.31	0.07, 0.003	-0.04, 0.11	0.00, 0.01	0.00, 0.01	0.06, 0.01	-0.03, 0.01
L	SupraMarginal Gyrus/Postcentral Gyrus/Inferior Parietal Lobule	305	-60	-18	38	2.83	0.52	0.04, 0.024	-0.05, 0.002	0.04, 0.04	0.08, 0.04	0.08, 0.04	0.03, 0.04
L	Cerebellum	247	-29	-75	-38	2.64	0.31	-0.04, 0.074	0.07, 0.004	0.02, 0.01	0.01, 0.01	0.01, 0.01	0.07, 0.02
L	Inferior Parietal Lobule/Middle Occipital Gyrus/Superior Parietal Lobule/Angular Gyrus	182	-31	-59	39	2.53	0.21	-0.05, 0.03	0.04, 0.09	0.00, 0.02	-0.02, 0.03	-0.04, 0.03	0.00, 0.03
R	Postcentral Gyrus/SupraMarginal Gyrus/Inferior Parietal Lobule/Precentral Gyrus/Middle Frontal Gyrus/Superior Parietal Lobule	166	55	-22	51	2.73	0.38	0.05, 0.03	-0.03, 0.17	0.05, 0.01	0.06, 0.02	0.08, 0.01	0.04, 0.02
L/R	Middle Cingulate Cortex/Precuneus/Posterior Cingulate Cortex	150	6	-42	23	2.52	0.24	-0.07, 0.001	0.04, 0.06	0.05, 0.01	0.04, 0.01	0.02, 0.01	0.06, 0.01
L	Middle Occipital Gyrus/Inferior Parietal Lobule/	124	-33	-85	32	2.89	0.47	-0.08, <0.001	0.03, 0.064	0.08, 0.03	0.08, 0.03	0.01, 0.03	0.12, 0.04
R	Superior Frontal Gyrus/Middle Frontal Gyrus	106	26	57	30	2.71	0.44	0.04, 0.04	-0.04, 0.04	-0.02, 0.04	-0.01, 0.03	0.02, 0.04	-0.05, 0.04
L/R	Precuneus	91	2	-57	44	2.58	0.32	-0.08, 0.001	0.03, 0.19	0.02, 0.05	0.01, 0.05	-0.06, 0.05	0.04, 0.05
R	Cerebellum	82	39	-69	-46	2.58	0.32	-0.03, 0.32	0.07, 0.008	-0.03, 0.04	0.00, 0.04	-0.01, 0.05	0.01, 0.04
L	Inferior Frontal Gyrus (p. Orbitalis)/Insula Lobe	81	-32	21	-13	2.67	0.33	0.07, 0.03	-0.02, 0.54	0.09, 0.05	0.12, 0.05	0.15, 0.06	0.11, 0.06
R	Superior Frontal Gyrus/Middle Frontal Gyrus	70	22	28	39	2.81	0.39	-0.09, 0.001	0.03, 0.20	-0.01, 0.06	-0.04, 0.05	-0.06, 0.06	0.00, 0.05
L	Inferior Frontal Gyrus (p. Triangularis)/Middle Frontal Gyrus/Inferior Frontal Gyrus (p. Opercularis)	69	-46	20	31	2.65	0.32	-0.09, 0.001	0.01, 0.83	0.00, 0.03	-0.02, 0.03	-0.06, 0.03	-0.03, 0.03
L	Middle Occipital Gyrus	43	-41	-88	7	3.02	0.51	0.05, 0.05	-0.07, 0.008	0.03, 0.02	0.04, 0.02	0.07, 0.02	-0.02, 0.02

Table S1 (cont.). Differential Amygdala Connectivity Changes by Treatment Arm

Hem.	MNI Atlas Region(s)	# Voxels	X	Y	Z	Voxel Stats		Extractions		Predicted Connectivity (mean, SD)			
						FDR Z		*Parameter, Significance*		Pre		Post	
						Mean	*SD*	*PE*	*WL*	PE	WL	PE	WL
L	Superior Orbital Gyrus/Olfactory cortex/Rectal Gyrus/ParaHippocampal Gyrus/Inferior Frontal Gyrus (p. Orbitalis)	42	-9	6	-15	2.59	0.27	0.07, 0.014	-0.04, 0.14	0.23, 0.04	0.24, 0.03	0.28, 0.05	0.20, 0.03
L	Postcentral Gyrus/Superior Parietal Lobule	36	-19	-48	73	2.84	0.42	0.02, 0.43	-0.08, 0.002	0.03, 0.01	0.03, 0.01	0.04, 0.01	-0.02, 0.01
L	Precuneus/Cuneus/Calcarine Gyrus	35	-13	-53	17	2.52	0.22	-0.09, <0.001	0.01, 0.63	0.07, 0.01	0.06, 0.01	0.02, 0.01	0.06, 0.01
L	Cerebellum	34	-26	-41	-42	2.88	0.43	-0.04, 0.09	0.08, 0.003	0.02, 0.02	0.01, 0.02	-0.01, 0.02	0.08, 0.02
R	Superior Temporal Gyrus/SupraMarginal Gyrus	25	60	-34	21	2.44	0.15	0.07, 0.04	-0.06, 0.10	0.06, 0.04	0.09, 0.05	0.09, 0.04	0.07, 0.05
L	Cerebellum	24	-7	-55	-46	2.48	0.18	-0.06, 0.03	0.08, 0.006	0.09, 0.01	0.09, 0.01	0.04, 0.01	0.14, 0.01
R	Fusiform Gyrus/Inferior Temporal Gyrus/Medial Temporal Pole	23	29	1	-33	2.49	0.15	0.07, 0.03	-0.05, 0.13	0.26, 0.04	0.27, 0.04	0.31, 0.05	0.23, 0.04
L	Fusiform Gyrus/ Cerebellum/Inferior Occipital Gyrus	23	-26	-68	-13	2.42	0.16	0.05, 0.11	-0.06, 0.07	0.06, 0.01	0.07, 0.01	0.10, 0.02	0.03, 0.01
L	Precentral Gyrus/Inferior Frontal Gyrus (p. Opercularis)	23	-39	1	32	2.41	0.13	-0.07, 0.01	0.03, 0.33	0.03, 0.03	0.02, 0.05	-0.02, 0.04	0.06, 0.05
L	Cuneus/Calcarine Gyrus	21	-6	-81	15	2.45	0.18	0.06, 0.03	-0.05, 0.05	0.00, 0.04	0.01, 0.04	0.05, 0.04	-0.03, 0.04
L	Middle Frontal Gyrus/Superior Frontal Gyrus	21	-25	27	33	2.72	0.36	-0.08, 0.001	0.03, 0.24	-0.03, 0.07	-0.08, 0.05	-0.09, 0.06	-0.04, 0.05
L	Lingual Gyrus/Precuneus/Calcarine Gyrus/Cerebellum/Posterior Cingulate Cortex	20	-9	-45	4	2.71	0.35	-0.10, <0.001	0.02, 0.47	0.13, 0.04	0.11, 0.03	0.08, 0.05	0.13, 0.03
R	Precentral Gyrus/Middle Frontal Gyrus	20	36	-4	47	2.50	0.19	0.08, 0.004	0.00, 0.86	-0.01, 0.04	0.02, 0.06	0.03, 0.05	0.02, 0.06
R	Olfactory cortex/Superior Orbital Gyrus/Rectal Gyrus/Inferior Frontal Gyrus (p. Orbitalis)	12	11	11	-15	2.45	0.16	0.05, 0.03	-0.04, 0.11	0.18, 0.04	0.18, 0.05	0.22, 0.05	0.14, 0.05

X, Y, and Z values are cluster center of mass coordinates in MNI stereotactic space; Voxel stats column depicts the mean and standard deviation of the voxelwise statistics for each clustered effect; Extractions column reports the mixed model parameter and significance value using extracted individual cluster beta values for each subject, specifying the slope of connectivity change within each treatment arm; Predicted connectivity column lists the summary statistics (mean and standard deviation) by group and time point for each individual's predicted level of connectivity derived from the mixed model; # = number; FDR = false discovery rate; Hem = hemisphere; L = left; MNI = Montreal Neurological Institute; PE = prolonged exposure treatment group; R = right; SD = standard deviation; WL = waiting list group.

Table S2. Differential Insula Connectivity Changes by Treatment Arm

Hem.	MNI Atlas Region(s)	# Voxels	X	Y	Z	Voxel Stats		Extractions		Predicted Connectivity (mean, SD)			
						FDR Z		*Parameter, Significance*		Pre		Post	
						Mean	*SD*	*PE*	*WL*	PE	WL	PE	WL
L/R	Cerebellum/Inferior Occipital Gyrus/Middle Occipital Gyrus/Lingual Gyrus/Calcarine Gyrus/Fusiform Gyrus/Superior Occipital Gyrus	5642	2	-72	-33	3.03	0.64	-0.04, <0.001	0.01, 0.22	0.01, 0.04	-0.03, 0.04	-0.02, 0.04	-0.01, 0.04
R	Hippocampus/ParaHippocampal Gyrus/Thalamus/Medial Temporal Pole/Amygdala/Cerebellum/Lingual Gyrus/Fusiform Gyrus/Inferior Temporal Gyrus/Putamen/Temporal Pole/Precuneus/ Caudate Nucleus/Posterior Cingulate Cortex/ Olfactory cortex	1997	13	-11	-7	2.92	0.57	0.05, <0.001	-0.04, <0.001	0.08, 0.02	0.09, 0.02	0.11, 0.02	0.06, 0.02
R	Inferior Frontal Gyrus (p. Triangularis)/Middle Frontal Gyrus/Inferior Frontal Gyrus (p. Orbitalis)/Inferior Frontal Gyrus (p. Opercularis)/Precentral Gyrus/Superior Orbital Gyrus/Middle Orbital Gyrus/Rectal Gyrus/Olfactory cortex	1485	38	22	16	2.81	0.41	0.03, 0.006	-0.04, 0.001	0.07, 0.03	0.09, 0.03	0.09, 0.03	0.05, 0.03
L	Precuneus/Superior Parietal Lobule/Lingual Gyrus/Calcarine Gyrus/Inferior Parietal Lobule/Cuneus/Superior Occipital Gyrus/Inferior Occipital Gyrus/Paracentral Lobule/Middle Cingulate Cortex/Postcentral Gyrus/Fusiform Gyrus/Middle Occipital Gyrus	1479	-11	-60	39	2.81	0.48	-0.05, <0.001	0.03, 0.007	0.05, 0.01	0.05, 0.02	0.01, 0.02	0.08, 0.02
L	Inferior Temporal Gyrus/Fusiform Gyrus/Medial Temporal Pole/Middle Temporal Gyrus/ParaHippocampal Gyrus/Hippocampus/Amygdala	1255	-45	-5	-31	2.93	0.56	0.03, 0.01	-0.05, <0.001	0.00, 0.04	0.02, 0.03	0.02, 0.04	-0.01, 0.03
L	Precentral Gyrus/Postcentral Gyrus/Inferior Frontal Gyrus (p. Opercularis)/Middle Frontal Gyrus/Inferior Frontal Gyrus (p. Triangularis)/Inferior Parietal Lobule	891	-53	-2	42	2.94	0.56	0.03, 0.01	-0.02, 0.14	0.07, 0.03	0.10, 0.03	0.11, 0.04	0.08, 0.04
R	Superior Frontal Gyrus/Superior Medial Gyrus/Superior Orbital Gyrus/Middle Frontal Gyrus/Mid Orbital Gyrus/Middle Orbital Gyrus	526	18	65	11	2.97	0.59	0.05, <0.001	-0.04, 0.004	0.01, 0.02	0.01, 0.02	0.05, 0.02	-0.02, 0.02
R	Superior Frontal Gyrus/Precentral Gyrus/Paracentral Lobule/SMA/Middle Frontal Gyrus/Postcentral Gyrus	517	18	-20	67	2.81	0.44	-0.06, <0.001	0.01, 0.30	0.03, 0.03	0.03, 0.03	-0.01, 0.03	0.04, 0.03
R	Inferior Temporal Gyrus/Middle Temporal Gyrus	420	58	-35	-13	2.92	0.62	0.01, 0.35	-0.08, <0.001	0.02, 0.05	0.04, 0.04	0.02, 0.04	-0.03 0.04
L	Middle Frontal Gyrus/Middle Orbital Gyrus/Superior Frontal Gyrus/Superior Orbital Gyrus	344	-32	51	10	3.04	0.69	-0.04, 0.03	0.01, 0.50	0.09, 0.01	0.08, 0.02	0.06, 0.01	0.08, 0.02

Table S2. (cont.) Differential Insula Connectivity Changes by Treatment Arm

Hem.	MNI Atlas Region(s)	# Voxels	X	Y	Z	Voxel Stats		Extractions		Predicted Connectivity (mean, SD)			
						FDR Z		*Parameter, Significance*		Pre		Post	
						Mean	*SD*	*PE*	*WL*	PE	WL	PE	WL
R	Postcentral Gyrus/Superior Parietal Lobule/Precentral Gyrus/Precuneus	327	24	-44	63	2.78	0.41	-0.04, 0.012	0.04, 0.007	0.07, 0.05	0.05, 0.04	0.04, 0.04	0.09, 0.04
L/R	Superior Medial Gyrus/Middle Cingulate Cortex/Anterior Cingulate Cortex/Superior Frontal Gyrus/SMA	299	-1	22	40	2.86	0.47	-0.02, 0.29	0.04, 0.026	0.16, 0.04	0.15, 0.03	0.14, 0.05	0.19, 0.03
L/R	Olfactory cortex/Rectal Gyrus/Inferior Frontal Gyrus (p. Orbitalis)/Superior Orbital Gyrus/Caudate Nucleus/Mid Orbital Gyrus/ Anterior Cingulate Cortex	266	-6	15	-11	2.83	0.49	0.07, <0.001	-0.05, 0.004	0.09, 0.09	0.10, 0.08	0.13, 0.08	0.06, 0.06
R	Middle Frontal Gyrus/Precentral Gyrus/Inferior Frontal Gyrus (p. Opercularis)	247	46	7	53	2.85	0.49	0.03, 0.09	-0.03, 0.12	0.07, 0.06	0.08, 0.05	0.10, 0.06	0.05, 0.05
R	Superior Parietal Lobule/Inferior Parietal Lobule/Postcentral Gyrus	244	36	-54	56	2.83	0.40	0.00, 0.98	-0.07,<0.001	0.01, 0.07	0.05, 0.07	0.00, 0.07	0.00, 0.08
L	Putamen/Amygdala	206	-28	-3	3	2.82	0.42	0.04, 0.04	-0.03, 0.10	0.25, 0.10	0.26, 0.11	0.28, 0.10	0.24, 0.10
L	Middle Frontal Gyrus/Superior Frontal Gyrus	202	-25	35	33	3.06	0.65	-0.04, 0.15	0.06, 0.007	0.10, 0.07	0.05, 0.05	0.08, 0.08	0.10, 0.09
L	Middle Frontal Gyrus/Superior Frontal Gyrus	190	-24	12	48	3.19	0.61	-0.08, <0.001	0.02, 0.28	-0.05, 0.04	-0.06, 0.04	-0.11, 0.04	-0.05, 0.04
L	Paracentral Lobule/Precentral Gyrus/SMA	151	-12	-24	68	2.89	0.50	-0.05, 0.003	0.04, 0.013	0.01, 0.05	0.01, 0.04	-0.04, 0.04	0.06, 0.05
R	Precentral Gyrus/Middle Frontal Gyrus/Postcentral Gyrus	148	54	-11	50	2.82	0.40	0.04, 0.06	-0.03, 0.15	0.10, 0.04	0.12, 0.03	0.14, 0.03	0.08, 0.03
R	Middle Occipital Gyrus/Angular Gyrus/Superior Occipital Gyrus/Middle Temporal Gyrus	143	39	-66	28	2.97	0.72	0.04, 0.06	-0.04, 0.03	-0.05, 0.08	-0.04, 0.08	-0.01, 0.08	-0.07, 0.08
L	Superior Frontal Gyrus/Middle Frontal Gyrus/SMA	141	-21	0	68	2.85	0.53	-0.06, 0.002	0.04, 0.016	0.05, 0.05	0.03, 0.04	0.00, 0.05	0.07, 0.05
L	Superior Orbital Gyrus	128	-20	65	-9	3.43	0.83	0.06, <0.001	-0.03, 0.05	0.00, 0.03	0.01, 0.03	0.07, 0.03	-0.03, 0.03
R	Calcarine Gyrus/Lingual Gyrus/Superior Occipital Gyrus/Inferior Occipital Gyrus/Cuneus	124	16	-99	-6	3.17	0.71	0.04, 0.017	-0.03, 0.112	0.03, 0.03	0.03, 0.03	0.07, 0.04	-0.01, 0.03
R	Calcarine Gyrus/Lingual Gyrus/Precuneus/Cuneus	118	16	-54	12	2.70	0.38	0.05, 0.014	-0.02, 0.38	0.08, 0.08	0.06, 0.06	0.15, 0.07	0.05, 0.06
L	Superior Frontal Gyrus/Superior Medial Gyrus	107	-18	66	15	3.46	0.85	0.03, 0.10	-0.05, 0.007	0.00, 0.03	0.01, 0.03	0.03, 0.04	-0.04, 0.03
L/R	Anterior Cingulate Cortex	98	-4	30	16	2.77	0.38	-0.04, 0.09	0.01, 0.66	0.23, 0.04	0.22, 0.03	0.19, 0.04	0.23, 0.03
L	Middle Frontal Gyrus/Superior Frontal Gyrus	92	-32	54	27	2.76	0.35	0.09, <0.001	-0.03, 0.11	0.11, 0.01	0.11, 0.01	0.18, 0.01	0.08, 0.01

Table S2. (cont.) Differential Insula Connectivity Changes by Treatment Arm

Hem.	MNI Atlas Region(s)	# Voxels	X	Y	Z	Voxel Stats		Extractions		Predicted Connectivity (mean, SD)			
						FDR Z		*Parameter, Significance*		Pre		Post	
						Mean	*SD*	*PE*	*WL*	PE	WL	PE	WL
R	Middle Frontal Gyrus	86	35	43	40	2.75	0.42	0.06, 0.005	0.01, 0.77	0.07, 0.04	0.05, 0.04	0.15, 0.04	0.05, 0.04
R	Superior Frontal Gyrus/Middle Frontal Gyrus	83	25	46	28	2.58	0.24	-0.04, 0.03	0.04, 0.04	0.17, 0.04	0.16, 0.04	0.14, 0.04	0.19, 0.05
L	Middle Frontal Gyrus/Inferior Frontal Gyrus (p. Triangularis)	79	-42	25	32	2.65	0.29	-0.07, 0.005	0.02, 0.37	0.03, 0.09	0.02, 0.09	-0.04, 0.09	0.04, 0.09
R	Cuneus	74	6	-84	25	2.70	0.36	0.05, 0.01	-0.04, 0.04	0.10, 0.04	0.11, 0.05	0.15, 0.05	0.08, 0.05
L	Cerebellum	56	-12	-65	-23	2.58	0.26	-0.06, 0.003	0.03, 0.10	0.08, 0.01	0.08, 0.02	0.04, 0.01	0.10, 0.02
R	Rectal Gyrus	53	6	56	-25	2.97	0.51	0.05, 0.004	-0.02 0.31	-0.02, 0.03	-0.02, 0.03	0.02, 0.03	-0.05, 0.03
R	SupraMarginal Gyrus/Superior Temporal Gyrus/Angular Gyrus	44	51	-42	22	2.50	0.17	0.06, 0.02	-0.04, 0.14	0.21, 0.08	0.19, 0.07	0.25, 0.08	0.16, 0.08
L	Middle Temporal Gyrus/SupraMarginal Gyrus/Angular Gyrus/Superior Temporal Gyrus	38	-49	-49	19	2.57	0.23	-0.08, 0.002	0.00, 0.91	0.18, 0.09	0.14, 0.09	0.11, 0.09	0.14, 0.09
R	Hippocampus/ParaHippocampal Gyrus	35	24	-38	-9	2.50	0.20	0.05, 0.01	-0.03, 0.17	0.10, 0.08	0.10, 0.07	0.15, 0.07	0.08, 0.07
R	Inferior Temporal Gyrus	34	57	2	-32	2.64	0.31	0.04, 0.03	-0.01, 0.53	-0.05, 0.02	-0.04, 0.02	-0.02, 0.02	-0.05, 0.02
L	Inferior Parietal Lobule/Angular Gyrus	33	-43	-52	43	2.60	0.26	-0.07, 0.008	0.01, 0.67	0.01, 0.10	-0.03, 0.08	-0.05, 0.13	-0.01, 0.08
L/R	Calcarine Gyrus/Cuneus	32	4	-97	9	2.93	0.47	-0.05, 0.003	0.03, 0.06	0.03, 0.01	0.04, 0.01	-0.02, 0.01	0.06, 0.01
R	Precentral Gyrus/Middle Frontal Gyrus	32	34	-8	47	2.57	0.23	0.08, 0.001	-0.01, 0.68	0.10, 0.03	0.11, 0.03	0.15, 0.03	0.11, 0.03

X, Y, and Z values are cluster center of mass coordinates in MNI stereotactic space; Voxel stats column depicts the mean and standard deviation of the voxelwise statistics for each clustered effect; Extractions column reports the mixed model parameter and significance value using extracted individual cluster beta values for each subject, specifying the slope of connectivity change within each treatment arm; Predicted connectivity column lists the summary statistics (mean and standard deviation) by group and time point for each individual's predicted level of connectivity derived from the mixed model; # = number; FDR = false discovery rate; Hem = hemisphere; L = left; MNI = Montreal Neurological Institute; PE = prolonged exposure treatment group; R = right; SD = standard deviation; WL = waitlist group.

Table S3. Differential Insula Connectivity Changes by Subregion and Treatment Arm

Hem.	MNI Atlas Region(s)	# Voxels	X	Y	Z	Voxel Stats		Extractions		Predicted Connectivity (mean, SD)			
						FDR Z		*Parameter, Significance*		Pre		Post	
						Mean	*SD*	*PE*	*WL*	PE	WL	PE	WL
						Dorsal Anterior Insula							
L	Precentral Gyrus/Postcentral Gyrus	248	-51	-7	45	2.66	0.29	0.04, 0.05	-0.01, 0.44	0.04, 0.06	0.09, 0.07	0.09, 0.05	0.07, 0.08
L	SupraMarginal Gyrus/ Inferior Parietal Lobule/ Angular Gyrus	201	-53	-50	31	2.67	0.32	-0.07, 0.003	0.06, 0.006	0.19, 0.13	0.18, 0.09	0.11, 0.11	0.25, 0.09
R	Superior Temporal Gyrus/SupraMarginal Gyrus	88	65	-31	23	2.71	0.31	0.07, 0.003	-0.01, 0.60	0.26, 0.12	0.25, 0.11	0.33, 0.12	0.24, 0.11
L/R	Anterior Cingulate Cortex/Superior Medial Gyrus	54	-1	36	19	2.44	0.15	-0.04, 0.18	-0.01, 0.73	0.23, 0.10	0.21, 0.08	0.21, 0.09	0.19, 0.08
R	SMA	44	10	21	66	2.45	0.20	-0.04, 0.04	0.03, 0.21	0.10, 0.08	0.07, 0.07	0.05, 0.09	0.10, 0.07
L	Precentral Gyrus/Inferior Frontal Gyrus (p. Opercularis)	42	-42	-2	31	2.56	0.26	-0.02, 0.39	0.04, 0.09	0.08, 0.08	0.12, 0.08	0.07, 0.07	0.14, 0.09
R	Middle Temporal Gyrus	25	50	-54	8	2.56	0.22	0.04, 0.16	0.02, 0.38	0.18, 0.11	0.16, 0.12	0.23, 0.09	0.19, 0.11
R	Cerebellum	23	19	-42	-23	2.44	0.16	0.08, <0.001	0.06, 0.004	0.03, 0.06	0.02, 0.07	0.11, 0.06	0.07, 0.07
						Posterior Insula							
L	Precentral Gyrus/Postcentral Gyrus	248	-51	-7	45	2.66	0.29	0.08, <0.001	-0.04, 0.04	0.17, 0.06	0.22, 0.07	0.27, 0.05	0.19, 0.07
L	SupraMarginal Gyrus/ Inferior Parietal Lobule/ Angular Gyrus	201	-53	-50	31	2.67	0.32	-0.02, 0.27	-0.01, 0.53	0.02, 0.13	0.01, 0.09	-0.02, 0.11	0.00, 0.09
R	Superior Temporal Gyrus/SupraMarginal Gyrus	88	65	-31	23	2.71	0.31	-0.07, 0.002	0.04, 0.04	0.28, 0.12	0.26, 0.10	0.20, 0.11	0.31, 0.11
L/R	Anterior Cingulate Cortex/Superior Medial Gyrus	54	-1	36	19	2.44	0.15	-0.07, 0.007	0.03, 0.25	0.14, 0.10	0.11, 0.08	0.08, 0.09	0.13, 0.08
R	SMA	44	10	21	66	2.45	0.20	-0.03, 0.15	0.01, 0.71	-0.09, 0.08	-0.12, 0.07	-0.14, 0.09	-0.12, 0.07
L	Precentral Gyrus/Inferior Frontal Gyrus (p. Opercularis)	42	-42	-2	31	2.56	0.26	0.07, 0.005	0.01, 0.78	0.12, 0.08	0.16, 0.08	0.19, 0.07	0.16, 0.08
R	Middle Temporal Gyrus	25	50	-54	8	2.56	0.22	0.11, <0.001	-0.02, 0.43	0.15, 0.10	0.13, 0.11	0.28, 0.07	0.11, 0.11
R	Cerebellum	23	19	-42	-23	2.44	0.16	0.06, 0.004	0.02, 0.37	0.14, 0.06	0.14, 0.07	0.21, 0.06	0.15, 0.07
						Ventral Anterior Insula							
L	Precentral Gyrus/Postcentral Gyrus	248	-51	-7	45	2.66	0.29	0.02, 0.19	0.01, 0.45	0.01, 0.06	0.06, 0.07	0.05, 0.05	0.07, 0.07
L	SupraMarginal Gyrus/ Inferior Parietal Lobule/ Angular Gyrus	201	-53	-50	31	2.67	0.32	-0.02, 0.45	-0.01, 0.80	0.15, 0.13	0.14, 0.09	0.12, 0.11	0.14, 0.09
R	Superior Temporal Gyrus/SupraMarginal Gyrus	88	65	-31	23	2.71	0.31	0.01, 0.52	-0.01, 0.68	0.13, 0.12	0.12, 0.10	0.14, 0.11	0.11, 0.11
L/R	Anterior Cingulate Cortex/Superior Medial Gyrus	54	-1	36	19	2.44	0.15	0.01, 0.70	-0.03, 0.22	0.30, 0.10	0.27, 0.08	0.32, 0.09	0.23, 0.08
R	SMA	44	10	21	66	2.45	0.20	0.01, 0.62	0.01, 0.47	0.09, 0.08	0.06, 0.07	0.08, 0.09	0.07, 0.07

L	Precentral Gyrus/Inferior Frontal Gyrus (p. Opercularis)	42	-42	-2	31	2.56	0.26	-0.01, 0.70	0.06, 0.005	-0.03, 0.08	0.00, 0.08	-0.04, 0.07	0.07, 0.08
R	Middle Temporal Gyrus	25	50	-54	8	2.56	0.22	-0.02, 0.37	0.01, 0.56	0.12, 0.11	0.10, 0.11	0.11, 0.08	0.12, 0.11
R	Cerebellum	23	19	-42	-23	2.44	0.16	-0.02, 0.43	0.04, 0.08	0.12, 0.06	0.11, 0.07	0.11, 0.06	0.14, 0.07

Table is separated by insula subregion and displays the treatment arm x time effects for each; X, Y, and Z values are cluster center of mass coordinates in MNI stereotactic space; Voxel stats column depicts the mean and standard deviation of the voxelwise statistics for each clustered effect; Extractions column reports the mixed model parameter and significance value using extracted individual cluster beta values for each subject, specifying the slope of connectivity change within each treatment arm; Predicted connectivity column lists the summary statistics (mean and standard deviation) by group and time point for each individual's predicted level of connectivity derived from the mixed model; # = number; FDR = false discovery rate; Hem = hemisphere; L = left; MNI = Montreal Neurological Institute; PE = prolonged exposure treatment group; R = right; SD = standard deviation; WL = waitlist group.

Table S4. Conjunction Analysis of Amygdala and Insula Treatment Arm x Time Effects

Hem.	MNI Atlas Region(s)	# Voxels	X	Y	Z
	Amygdala and Insula Shared Connectivity Increases from Pre- to Post-Treatment for PE vs. WL				
R	Superior Frontal Gyrus/ Middle Frontal Gyrus	67	22	60	28
L	Postcentral Gyrus	66	-58	-18	46
L/R	Cuneus	54	6	-83	25
R	Precentral Gyrus/Postcentral Gyrus	36	57	-13	51
L	Superior Orbital Gyrus/Rectal Gyrus/Inferior Frontal Gyrus (p. Orbitalis)	10	-11	9	-15
	Amygdala and Insula Shared Connectivity Decreases from Pre- to Post-Treatment for PE vs. WL				
L	Cerebellum	38	-28	-72	-38
L	Inferior Parietal Lobule/Superior Parietal Lobule	24	-29	-53	41
L	Inferior Frontal Gyrus (p. Triangularis)/Middle Frontal Gyrus	10	-43	21	32

Table is separated by shared increases and shared decreases in connectivity for the conjunction of the amygdala and insula FDR-corrected time x treatment arm statistical maps; X, Y, and Z values are cluster center of mass coordinates in MNI stereotactic space; FDR = false discovery rate; Hem = hemisphere; L = left; MNI = Montreal Neurological Institute; PE = prolonged exposure treatment group; R = right; WL = waitlist group.

Table S5. Peak Loci of Maximal Low-Frequency BOLD Signal Fluctuations of Bilateral Amygdala and Insula

Hem.	Region	X	Y	Z
L	Amygdala	-22	-6	-18
R	Amygdala	20	-6	-16
L	Insula	-44	10	-2
R	Insula	46	13	-2

Table indicates peak MNI coordinates of maximal low-frequency BOLD signal fluctuations in the left and right amygdala and insula (anatomically constrained utilizing seed region masks) identified via a general linear model fitting of a cosine basis set to the pre-processed resting state signals and defined utilizing an F contrast across all regressors of interest; Single-subject foci were determined via defining a 6 mm radius sphere around each above focus and identifying the peak voxel for each participant of the F contrast of interest within this 6 mm sphere, with the result single-subject peaks having the principal eigenvariate of the BOLD signal time course extracted from a 6mm radius sphere centered around this single-subject peak for use in DCM analyses; X, Y, and Z values are cluster center of mass coordinates in MNI stereotactic space; BOLD = blood oxygenation-level dependent; DCM = dynamic causal modeling; Hem = hemisphere; L = left; MNI = Montreal Neurological Institute; R = right.

Table S6. Effective Connectivity Parameters of DCM Network at Baseline.

Connection	Parameter Estimate (Hz)	Posterior Probability
Left Amygdala to Right Amygdala	0.389	1.00
Left Amygdala to Left Insula	-0.453	1.00
Left Amygdala to Right Insula	-0.482	1.00
Left Amygdala to Left Intraparietal Sulcus	-0.132	1.00
Right Amygdala to Left Amygdala	0.343	1.00
Right Amygdala to Left Insula	-0.261	1.00
Right Amygdala to Right Insula	-0.209	1.00
Right Amygdala to Left Inferior Frontal Junction	-0.174	1.00
Right Amygdala to Left Intraparietal Sulcus	-0.107	0.97
Left Insula to Left Amygdala	0.096	1.00
Left Insula to Left Insula (Inhibitory Self-Connection)	-0.306	1.00
Left Insula to Right Insula	0.217	1.00
Left Insula to Left Inferior Frontal Junction	0.100	1.00
Left Inferior Frontal Junction to Left Amygdala	-0.097	0.97
Left Inferior Frontal Junction to Right Amygdala	-0.099	0.98
Left Inferior Frontal Junction to Left Insula	-0.299	1.00
Left Inferior Frontal Junction to Right Insula	-0.310	1.00
Left Inferior Frontal Junction to Left Inferior Frontal Junction (Inhibitory Self-Connection)	-0.352	1.00
Left Intraparietal Sulcus to Left Insula	-0.345	1.00
Left Intraparietal Sulcus to Right Insula	-0.263	1.00
Left Intraparietal Sulcus to Left Inferior Frontal Junction	0.256	1.00
Left Intraparietal Sulcus to Left Intraparietal Sulcus (Inhibitory Self-Connection)	-0.439	1.00

Table reports the parameter estimates and posterior probabilities for DCM connections demonstrating strong evidence (posterior probability > 0.95) of being present (free energy of all nested models with vs. without the connection present) in the entire randomized PTSD sample at baseline; Parameters and posterior probabilities were obtained via parametric empirical Bayes of fully-specified first-level DCM models, with a subsequent post-hoc search across all nested models to determine the evidence of the presence or absence for each parameter; Positive parameters indicate an excitatory influence of the originator on the target, whereas negative parameters indicate an inhibitory influence of the originator on the target; DCM = dynamic causal modeling; Hz = hertz.

Table S7. Effective Connectivity Parameter Differential Modulation by Time (Post vs. Pre-Treatment) for Prolonged Exposure vs. Waiting List

Connection	Parameter Estimate (Hz)	Posterior Probability
Left Amygdala to Left Insula	0.102	1.00
Right Amygdala to Left Intraparietal Sulcus	0.084	1.00
Left Inferior Frontal Junction to Left Amygdala	0.074	1.00
Left Intraparietal Sulcus to Left Amygdala	-0.069	1.00

Table reports the parameter estimates and posterior probabilities for differential (prolonged exposure vs. waiting list) time-related (post vs. pre-treatment) modulation of DCM connections demonstrating strong evidence (posterior probability > 0.95) of being present (free energy of all nested models with vs. without the connection present) for the third-level parametric empirical Bayes model comparing time-related effects of second-level parametric empirical Bayes models within each treatment arm (prolonged exposure and waiting list); Parameters and posterior probabilities were obtained via third-level parametric empirical Bayes examining treatment arm as a modulator of second-level post vs. pre-treatment parametric empirical Bayes models within each treatment arm (prolonged exposure and waiting list, all based on fully-specified first-level DCM models), with a subsequent post-hoc search across all nested models to determine the evidence of the presence or absence for each parameter; Parameters indicate the difference in time-related effects (post- vs. pre-treatment) for prolonged exposure vs. waiting list, with positive parameters indicating a greater magnitude shift in the connection for prolonged exposure vs. waiting list towards more excitation/less inhibition, and negative parameters indicating a greater magnitude shift in the connection for prolonged exposure vs. waiting list towards less excitation/more inhibition at post- vs. pre-treatment; DCM = dynamic causal modeling; Hz = hertz.

Table S8. Effective Connectivity Parameter Modulation of Post vs. Pre-Treatment Changes for Prolonged Exposure by Reductions in CAPS Total Scores

Connection	Parameter Estimate (Hz)	Posterior Probability
Right Amygdala to Left Intraparietal Sulcus	-0.009	1.00
Left Inferior Frontal Junction to Left Amygdala	0.005	1.00
Left Intraparietal Sulcus to Left Amygdala	0.004	1.00

Table reports the parameter estimates and posterior probabilities for parameters specifying modulation of time-related (post vs. pre-treatment) changes in DCM connections in the prolonged exposure arm as a function of changes in CAPS total scores (pre- vs. post-treatment) which demonstrated strong evidence (posterior probability > 0.95) of being present (free energy of all nested models with vs. without the connection present) for the third-level parametric empirical Bayes model comparing the continuous relationship of time-related effects of a second-level parametric empirical Bayes model within the prolonged exposure group to observed changes in CAPS total scores from pre- to post-treatment; Parameters and posterior probabilities were obtained via third-level parametric empirical Bayes model of CAPS total score changes modulating the second-level post vs. pre-treatment parametric empirical Bayes model within the prolonged exposure arm (based on fully-specified first-level DCM models) with a subsequent post-hoc search across all nested models to determine the evidence of the presence or absence for each parameter; The parameter estimate indicates the degree of modulation of the time-related parameter shift by a per unit change in CAPS total score above or below the sample mean, with positive values indicating greater reductions in CAPS are associated with more of a shift towards greater excitation/less inhibition, and negative values indicating greater CAPS reductions are associated with more of a shift towards less excitation/more inhibition; DCM = dynamic causal modeling; Hz = hertz.